

# CHAPTER-2

# ELECTRONIC TRANSPORT IN GRAPHENE SYSTEMS AT ZERO TEMPERATURE

---

In this chapter, we report our investigations on electron-impurity scattering rate ( $\hbar/\tau$ ) as a function of quasiparticle energy ( $E$ ) and impurity concentration ( $n_i$ ) for doped monolayer graphene (MLG), bilayer graphene (BLG) and monolayer gapped graphene (MLGG) at zero temperature using Boltzmann transport equation and compare them with 2-dimensional electron gas (2DEG). ( $\hbar/\tau$ ) of MLG has been computed analytically as well as numerically. Computed results show that  $\hbar/\tau$  of MLG; (a) tends to zero at  $E = 0$  and, (b) it exhibits peak at  $\approx 1.56E_f$ , where  $E_f$  is Fermi energy. Contrary to this,  $\hbar/\tau$  of 2DEG, BLG and MLGG show their maximum values at  $E = 0$  and decline thereafter on increasing  $E$  to attain a minimum at around  $E$  equal to Fermi energy. We thus find that  $\hbar/\tau$  versus  $E$  of MLG displays an entirely different behaviour than that of BLG, MLGG and 2DEG, suggesting that electron-impurity scattering process in MLG sharply differs from those in BLG, MLGG and 2DEG. Further, computed  $\hbar/\tau$  of MLG exhibits a large variation in its magnitude over the energy range of  $0 \leq E \leq 3E_f$ . Estimation of conductivity ( $\sigma$ ) within Boltzmann transport theory involves an electron-impurity scattering rate averaged over all possible values of  $E$ . It can therefore be inferred that the computation of  $\sigma$  with the use of  $\hbar/\tau$  at  $E = E_f$  for comparing the computed results with experimental data can be highly misleading. We also investigate the  $\hbar/\tau$  changes drastically on introduction of energy gap in electronic states of graphene.  $\hbar/\tau$  versus  $E$  of MLGG exhibits drastic change in its behavior for lower values of  $E < E_f$  on increasing  $a$ . At higher values of  $a$  ( $\approx 0.9$ ) behavior of  $\hbar/\tau$  of MLGG is found to be similar to that of BLG. Magnitude of  $\hbar/\tau$  has been found to decline with increasing values

of  $a$ , at all values of  $E$ . Scattering rates of MLG, 2DEG, BLG, and MLGG are found increasing on enhancing the impurity concentration.

## 2.1 Introduction

There have been tremendous experimental and theoretical interests in monolayer graphene (MLG), bilayer graphene (BLG) and monolayer gapped graphene (MLGG) because of their novel physical properties and their use as enticing materials for electronics. MLG is a two dimensional (2D) system of carbon atoms covalently bonded together in a real space honey comb lattice that comprises of two interpenetrating triangular sublattices. It MLG has concomitant reciprocal space honey comb lattice with a hexagonal Brillouin zone that encompasses K-points. Near K-points, band structure is described by Dirac equation and the carriers follow linear chiral Dirac like energy dispersion relation, which can be written as;  $E_{sk}^{MLG} = s \hbar v_f |\mathbf{k}|$ , where  $\mathbf{k}$  is 2D wave vector and  $v_f$  ( $\approx 10^6$  m/s) is the Fermi velocity that does not dependent on carrier density,  $n$ . Because of its very large electron mean-free path, novel phenomenon like integral quantum Hall effect (IQHE) [1] can be observed in MLG and the ballistic transport at distances up to  $1 \mu m$  can be observed experimentally in MLG at room temperature [2]. It has been found that most of the observed transport properties of graphene sheets at zero magnetic fields can be explained with the use of theory of scattering from randomly distributed charged impurities and hence main mechanism of transport in MLG appears to be diffusion. Further, unlike metallic carbon nanotubes [3-8], back scattering has been found absent in Graphene giving raise charge-carrier mobility as high as up to  $15,000 \text{ cm}^2 \text{ V}^{-1} \text{ S}^{-1}$ , even under ambient conditions [1, 2, 9-11]. Because of zero-gap at Dirac points in the electronic spectrum of MLG, it is challenging to create graphene-based devices. However, recent experiments have demonstrated that a gap between valance band and conduction band can be opened [12-15]. On opening of gap, relativistic massless Dirac

particle dispersion relation changes to  $E_{sk}^{\text{MLGG}} = s\sqrt{(E_k)^2 + \Delta^2} = \sqrt{(\hbar v_F k)^2 + \Delta^2}$ . The extra intrinsic mass,  $\Delta = m v_F^2 = a \mu_f$ , is introduced due to a break in the graphene's sublattice symmetry. Here where  $\mu_f = \sqrt{(\hbar v_f k_f)^2 + \Delta^2}$  is chemical potential at absolute zero temperature and  $a$  is the gap constant having  $0 \leq a < 1$  when Fermi level is considered to lying above energy gap.

Another graphene system called BLG has the tunable energy band gap which is one of the most spectacular properties for device applications [16-20]. Charge transport in BLG differs qualitatively from that in MLG due to different energy dispersion and chiral function. In the case of BLG, energy dispersion relation is given by  $E_{sk}^{\text{BLG}} = s \hbar^2 k^2 / (2m)$ , with  $m = \gamma / (2 v_f^2) \approx 0.033 m_e$ ,  $\gamma \approx 0.39$  eV is the interlayer coupling constant [21]. The properties of BLG have been found intermediate between properties of MLG and regular 2DEG. Similar to the MLG, BLG shows zero band gap at the Dirac point (K and K' point), but has quadratic energy dispersion like that of 2DEG. Charge transport in BLG differs qualitatively from that in MLG.

One of the most prominent scattering processes that control the charge transport in MLG, BLG and MLGG is scattering of charge carriers from disorder or the randomly distributed impurities. Physics of disorder in graphene and how disorder affects the transport property has remained very tempting subject of investigations in graphene. Various scattering mechanisms for Dirac fermions in MLG, BLG and MLGG have been studied in past [22-24]. It is widely believed that electronic transport in graphene is most likely controlled by charge impurities and ripples (microscopic corrugations of a graphene sheet). Scattering due to short-range potential created by neutral impurities or by lattice defects is found mostly irrelevant in graphene. Charge carrier scattering from long range coulomb potential created by charged impurities in MLG, BLG and MLGG has recently been investigated by several

people [24-27]. These investigations suggest that coulomb scattering mainly limits the charge-carrier mobility in graphene samples. Results on changes in  $\sigma$  due to scattering from random charge impurity of concentration,  $n_i$  suggest that  $\sigma$  of MLG scales linearly with  $n_c/n_i$  and the mobility remains independent of the Fermi energy, which has been found in good agreement with experimental results [28].

Most of prior reported theoretical calculations on  $\sigma$  of graphene systems have been made using  $\hbar/\tau$  computed at Fermi energy [24-26, 28-30]. However,  $\sigma$  within Boltzmann transport theory is given by  $\sigma = (be^2/h) (E_f \langle \tau \rangle / \hbar)$  (where  $b$  is 2 for MLG and MLGG and is 4 for BLG) which involves  $1/\langle \tau \rangle$ , averaged value of  $1/\tau$  over all possible values of quasiparticle energy,  $E$ .  $1/\langle \tau \rangle$  can significantly differ from  $1/\tau$  at Fermi energy. Thus, the use of  $\hbar/\tau$  at Fermi energy for comparing computed  $\sigma$  with experimentally measured values can be grossly misleading. Further, the detailed understanding of process of  $\hbar/\tau$  can only be made by calculating  $\hbar/\tau$  for all possible values of  $E$ . This motivated us to calculate  $\hbar/\tau$  as a function of  $E$  for the doped MLG, BLG and MLGG at zero temperature. We performed both analytical as well as numerical calculations on scattering for MLG. To understand how  $\hbar/\tau$  in MLG differs from that of 2DEG, BLG, and MLGG, we computed  $\hbar/\tau$  for 2DEG, BLG, and MLGG. Our results suggest that  $\hbar/\tau$  of MLG sharply differs from that of 2DEG, BLG and MLGG and  $\hbar/\tau$  enhances on increasing impurity concentration ( $n_i$ ). This chapter is divided into 4 sections. Useful formalisms for MLG, 2DEG, BLG and MLGG are given in section-2.2. Results from our calculation are discussed in section-2.3 and the references are quoted in section-2.4.

## 2.2 Formalism

### 2.2.1 Static Polarization function of MLG, 2DEG, BLG, & MLGG

The static screening properties of the graphene based systems in the RPA are defined by the static dielectric function  $\epsilon(q)$ :

$$\epsilon(q) = 1 + v_i \Pi(q), \quad (2.1)$$

where  $v_i(q) = 2\pi e^2/(\kappa q)$  is random charge impurity potential with  $\kappa = 2.5$  is effective background dielectric constant of SiO<sub>2</sub> as a substrate material [25] and  $q$  is the momentum transfer to the scattered electron.  $\Pi(q)$  is the static polarization function is given by the bare bubble diagram;

$$\Pi(q) = \frac{g_s g_v}{A^2} \sum_{k s s'} \frac{f_{k s} - f_{k' s'}}{E_{k s} - E_{k' s'}} F_{s s'}(\mathbf{k}, \mathbf{k}'), \quad (2.2)$$

where  $g_v = 2$  is the valley degeneracy due to the  $\mathbf{k}$  and  $\mathbf{k}'$  points and  $g_s = 2$  is the spin degeneracy,  $\mathbf{k}' = \mathbf{k} + \mathbf{q}$ ,  $s(s') = +(-)$  denote the conduction (valance) band indices,  $E_{k s}$  is the energy which is defined as  $E_{s k}^{\text{MLG}} = s\gamma k$  for MLG,  $E_{s k}^{\text{BLG}} = s\hbar^2 k^2/(2m)$  for BLG and

$E_{s k}^{\text{MLGG}} = \mu_{s k} = s\sqrt{(\hbar v_F k)^2 + \Delta^2}$  for MLGG with  $\Delta = m v_f^2$  is the extra intrinsic mass.

$F(\mathbf{k}, \mathbf{k}')$  is the chirality function and it is defined as  $F_{s s'}^{\text{MLG}}(\mathbf{k}, \mathbf{k}') = (1 + s s' \cos \theta_{\mathbf{k} \mathbf{k}'})/2$  for

MLG,  $F_{s s'}^{2\text{DEG}}(\mathbf{k}, \mathbf{k}') = 1$  for 2DEG,  $F_{s s'}^{\text{BLG}}(\mathbf{k}, \mathbf{k}') = (1 + s s' \cos 2\theta_{\mathbf{k} \mathbf{k}'})/2$  for BLG, and

$F_{s s'}^{\text{MLGG}}(\mathbf{k}, \mathbf{k}') = \left( \left( \frac{E^2 + 2\Delta^2}{E^2 + \Delta^2} \right) + \left( \frac{E^2}{E^2 + \Delta^2} \right) \cos \theta_{\mathbf{k} \mathbf{k}'} \right) / 4$  for MLGG where  $\theta_{\mathbf{k} \mathbf{k}'} = \theta$  is the

scattering angle between  $\mathbf{k}$  and  $\mathbf{k}'$ .  $f_{s k} = [1 + \exp\{(E_{k s} - \mu_c)/k_B T\}]^{-1}$  is the Fermi distribution function with  $\mu_c$  is the chemical potential. In this chapter we defined zero

temperature static polarization function of extrinsic case (where  $n_c$  and  $E_f \neq 0$ ). At  $T = 0$ ,

$f_{-k} = 0$  and  $f_{+k} = \theta(k_f - |\mathbf{k}|)$  and we can write Eq. (1) as  $\Pi(q) = \Pi_{\text{Intra}}(q) + \Pi_{\text{Inter}}(q)$ ,

where

$$\Pi_{\text{Intra}}(q) = \frac{g_s g_v}{A^2} \sum_{k_s} \frac{f_{k_s} - f_{k'_s}}{E_{k_s} - E_{k'_s}} F_{SS}(\mathbf{k}, \mathbf{k}') \quad (2.3)$$

and

$$\Pi_{\text{Inter}}(q) = \frac{g_s g_v}{A^2} \sum_{k_s} \frac{f_{k_s} - f_{-k'_s}}{E_{k_s} - E_{-k'_s}} F_{-SS}(\mathbf{k}, \mathbf{k}'). \quad (2.4)$$

The polarization functions that are required to calculate  $\epsilon^{\text{MLG}}(q)$ ,  $\epsilon^{2\text{DEG}}(q)$ ,  $\epsilon^{\text{BLG}}(q)$ , and  $\epsilon^{\text{MLGG}}(q)$ , for MLG, 2DEG, BLG, and MLLG, respectively, have been calculated analytically within RPA. The calculated values are given by [33-36]

$$\frac{\Pi^{\text{MLG}}(q)}{N^{\text{MLG}}(E_f)} = \begin{cases} 1 & (q \leq 2k_f) \\ 1 - \frac{1}{2} \sqrt{1 - \left(\frac{2k_f}{q}\right)^2} - \frac{q}{4k_f} \sin^{-1}\left(\frac{2k_f}{q}\right) + \frac{\pi q}{8k_f} & (q > 2k_f) \end{cases} \quad (2.5)$$

$$\frac{\Pi^{2\text{DEG}}(q)}{N^{2\text{DEG}}(E_f)} = \begin{cases} 1 & (q \leq 2k_f) \\ 1 - \sqrt{1 - \left(\frac{2k_f}{q}\right)^2} & (q > 2k_f) \end{cases} \quad (2.6)$$

$$\frac{\Pi^{\text{BLG}}(q)}{N^{\text{BLG}}(E_f)} = \begin{cases} \frac{\sqrt{4k_f^4 + q^4}}{2k_f^2} - \ln\left(\frac{k_f^2 + \sqrt{k_f^4 + \frac{q^4}{4}}}{2k_f^2}\right) & (q \leq 2k_f) \\ \frac{\sqrt{4k_f^4 + q^4}}{2k_f^2} - \ln\left(\frac{k_f^2 + \sqrt{k_f^4 + \frac{q^4}{4}}}{2k_f^2}\right) - \frac{(2k_f^2 + q^2)\sqrt{q^4 - 4k_f^4}}{2k_f^2 q} - \ln\left(\frac{q - \sqrt{q^2 - 4k_f^2}}{q + \sqrt{q^2 - 4k_f^2}}\right) & (q > 2k_f) \end{cases} \quad (2.7)$$

and

$$\frac{\Pi^{\text{MLGG}}(q)}{N^{\text{MLGG}}(\mu_f)} = \begin{cases} 1 & (q \leq 2k_f) \\ 1 - \left\{ \frac{\sqrt{q^2 - 4k_f^2}}{2q} + \frac{E_f^2 - \Delta^2}{\gamma q \sqrt{E_f^2 + \Delta^2}} \tan^{-1}\left(\frac{\gamma \sqrt{q^2 - 4k_f^2}}{2\sqrt{E_f^2 + \Delta^2}}\right) \right\} & (q > 2k_f) \end{cases} \quad (2.8)$$

In the Eqs. (2.5)-(2.8),  $N^{\text{MLG}}(E_f)$ ,  $N^{2\text{DEG}}(E_f)$ ,  $N^{\text{BLG}}(E_f)$  and  $N^{\text{MLGG}}(\mu_f)$  are density of states at Fermi level for MLG, 2DEG, BLG, and MLGG, respectively, and define in next section.

## 2.2.2 Boltzmann Transport Equation for MLG, BLG, MLGG & 2DEG

The scattering rate for an electron in spin state  $s$ , scattered from disorder and or statically screened Coulomb potential at zero temperature, is given by [22, 27, 32]

$$\frac{\hbar}{\tau(E_{sk})} = 2\pi n_i \int \frac{d^2 k'}{(2\pi)^2} \left| \frac{v_i(q)}{\epsilon(q)} \right|^2 (1 - \cos \theta_{kk'}) F(k, k') \delta(E_{sk} - E_{sk'}), \quad (2.9)$$

where  $n_i$  is the impurity concentration. Simplification of integral in Eq. (1) for MLG, 2DEG, BLG, and MLGG respectively gives;

$$\frac{\hbar}{\tau^{\text{MLG}}(E)} = n_i N^{\text{MLG}}(E) \int_0^\pi \left( \frac{2\pi e^2}{k q \epsilon^{\text{MLG}}(q)} \right)^2 (1 - \cos \theta) \left( \frac{1}{2} \right) (1 + \cos \theta) d\theta, \quad (2.10)$$

$$\frac{\hbar}{\tau^{\text{2DEG}}(E)} = 2 n_i N^{\text{2DEG}}(E) \int_0^\pi \left( \frac{2\pi e^2}{k q \epsilon^{\text{2DEG}}(q)} \right)^2 (1 - \cos \theta) d\theta, \quad (2.11)$$

$$\frac{\hbar}{\tau^{\text{BLG}}(E)} = n_i N^{\text{BLG}}(E) \int_0^\pi \left( \frac{2\pi e^2}{k q \epsilon^{\text{BLG}}(q)} \right)^2 (1 - \cos \theta) \left( \frac{1}{2} \right) (1 + \cos 2\theta) d\theta, \quad (2.12)$$

and

$$\frac{\hbar}{\tau^{\text{MLGG}}(E)} = n_i N^{\text{MLGG}}(E) \int_0^\pi \left( \frac{2\pi e^2}{k q \epsilon^{\text{MLGG}}(q)} \right)^2 (1 - \cos \theta) \left( \frac{1}{4} \right) \left( \left( \frac{E^2 + 2\Delta^2}{E^2 + \Delta^2} \right) + \left( \frac{E^2}{E^2 + \Delta^2} \right) \cos \theta \right) d\theta. \quad (2.13)$$

In above equations,  $N^{\text{MLG}}(E)$ ,  $N^{\text{2DEG}}(E)$ ,  $N^{\text{BLG}}(E)$  and  $N^{\text{MLGG}}(E)$  are density of states for MLG, 2DEG, BLG and MLGG, respectively and these are defined as (see Appendix-A);

$$N^{\text{MLG}}(E) = g_s g_v \frac{|E|}{2\pi \gamma^2}, \quad (2.14)$$

$$N^{\text{2DEG}}(E) = g_v \frac{m}{\pi \hbar^2}, \quad (2.15)$$

$$N^{\text{BLG}}(E) = g_s g_v \frac{m}{\pi \hbar^2}, \quad (2.16)$$

and

$$N^{\text{MLGG}}(E) = g_s g_v \frac{\sqrt{E^2 + \Delta^2}}{2\pi \gamma^2}, \quad (2.17)$$

Where,  $\gamma = 6.46 \text{ eV \AA}$  is a band parameter,  $m$  is the effective mass of electron in 2DEG and BLG. Energy states, which are close to Fermi level, mainly contribute to the electronic conduction. Near the Fermi surface, conservation of energy ensures that we can take  $q = 2 (E/\gamma) \sin(\theta/2)$  for all practical purposes. Static dielectric function involves system specific effective screening of impurity potential. Thus, Eqs. (2.10) to (2.13) not only differ from each in  $\theta$ -dependent terms they have altogether different values of density of states and static dielectric functions. The term  $(1 - \cos \theta)$  is common in all four equations, which always appears in Boltzmann transport formalism. In the case of MLG, the probability of backward scattering at  $\theta = \pi$  vanishes due to the factor  $(1 + \cos \theta)$ . Contrary to this, backward scattering in the 2DEG plays key role in determining the transport property at low density and low temperature [31, 37]. Also, the backward scattering in the BLG is restored and even enhanced by the factor  $(1 + \cos 2\theta)$  because of the quadratic dispersion and, most critically, due to its chiral nature. The chiral factor  $\frac{1}{2} \left( \left( \frac{E^2 + 2\Delta^2}{E^2 + \Delta^2} \right) + \left( \frac{E^2}{E^2 + \Delta^2} \right) \cos \theta \right)$  for MLGG reduces to  $\frac{1}{2}(1 + \cos \theta)$  for  $\Delta = 0$  which is the case of MLG and 1 for  $\Delta \rightarrow \infty$  which is the case of 2DEG. Due to the qualitative difference in the dispersion relation and screening property between MLG and BLG, it is expected that the transport and other electronic property of BLG are more similar to the 2DEG than the MLG.

## 2.3 Results & Discussions

### 2.3.1 Static Polarization Function of MLG, BLG, MLGG & 2DEG

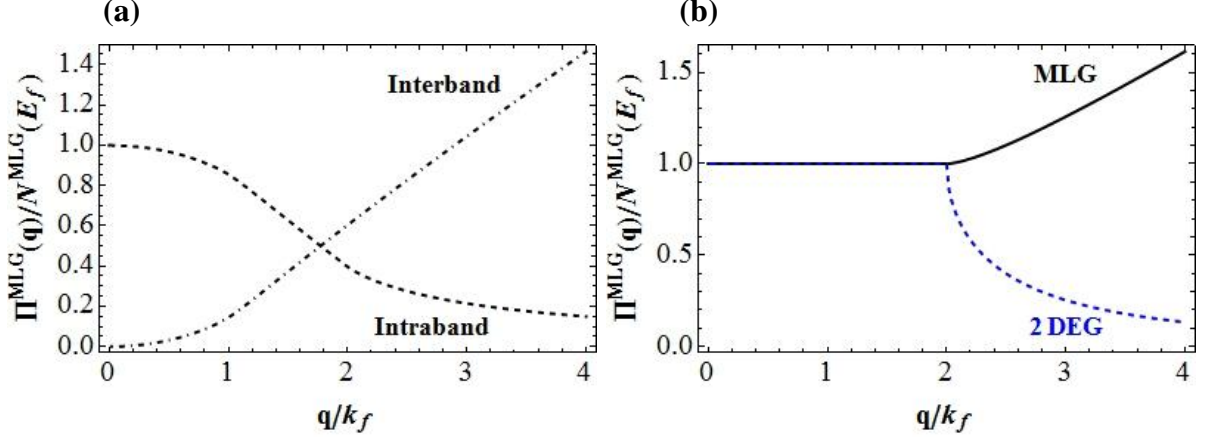


**Figure 2.1:** Calculated (a) Intraband (black-dashed) and interband (black-dot dashed) and (b) total (black-solid) static polarization function as a function of wave vector for MLG. Blue-dashed curve show the static polarization function of 2DEG.

In Fig. 2.1, we show the calculated static polarization function as a function of the wave vector for MLG. Figure 2.1 (a) shows the numerically calculated intraband (black-dashed) and interband (black-dot dashed) polarization functions, respectively, using Eqs. (2.3) and (2.4) for MLG. Figure 2.1 (b) shows the calculated total polarization function of MLG with those of 2DEG (Blue-dashed) for comparison. At  $q = 0$ , we have  $\Pi_{\text{Intra}}^{\text{MLG}}(q = 0) = N^{\text{MLG}}(E_f)$  and  $\Pi_{\text{Inter}}^{\text{MLG}}(q = 0) = 0$ . For  $q \leq 2k_f$ ,  $\Pi_{\text{Intra}}^{\text{MLG}}(q)$  and  $\Pi_{\text{Inter}}^{\text{MLG}}(q)$  decreases and increases, respectively, with  $q$  increases in a such way the total static polarizability becomes a constant i.e.  $\Pi^{\text{MLG}}(q) = \Pi_{\text{Intra}}^{\text{MLG}}(q) + \Pi_{\text{Inter}}^{\text{MLG}}(q) = N^{\text{MLG}}(E_f)$ . For  $q > 2k_f$ , the total polarization function of MLG increases linearly with  $q$  due to the interband transition as can be seen in Figure 2.1 (a). This is a very different behavior from 2DEG where the static polarization function falls off rapidly for  $q > 2k_f$  with a cusp at  $q = 2k_f$  [32]. Over all MLG screening is a mixing of metallic screening due to intraband and insulation screening due to interband.

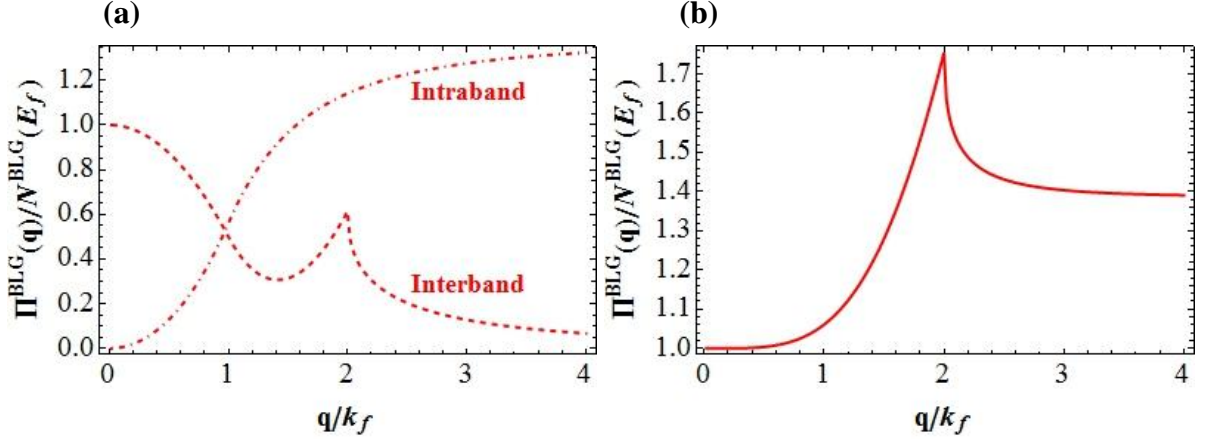


**Figure 2.2:** Calculated (a) Intraband (red-dashed) and interband (red-dot dashed) and (b) total (red-solid) static polarization function as a function of wave vector for BLG.

In Figure 2.2, we show the calculated static polarization function as a function of the wave vector. Figure 2.2 (a) shows the numerically calculated intraband (red-dashed) and interband (red-dot dashed) polarization functions, respectively, using Eqs. (2.3) and (2.4) for BLG. Figure 2.2 (b) shows total polarization functions of BLG. At  $q = 0$ , same as in the case of MLG,  $\Pi_{\text{intra}}^{\text{BLG}}(q = 0) = N^{\text{BLG}}(E_f)$  and  $\Pi_{\text{inter}}^{\text{BLG}}(q = 0) = 0$ , which follow also from the compressibility sum rule  $\Pi^{\text{BLG}}(q = 0) = \int dE [-df/dE] N^{\text{BLG}}(E)$ . For small  $q$ ,  $\Pi_{\text{intra}}^{\text{BLG}}$  decreases as  $1 - q^2/2k_f^2$ , and  $\Pi_{\text{inter}}^{\text{BLG}}$  increases as  $q^2/2k_f^2$ . This behavior comes from the overlap factor  $F_{ss'}^{\text{BLG}}$  in Eqs. (2.3) and (2.4). However, for BLG, the cancellation of two polarization functions is not exact especially for  $q > k_f$  because of the enhanced backscattering, so the total polarization function increases as  $q$  approaches  $2k_f$ , which means screening increases as  $q$  increases. Thus BLG, in spite of being a 2D system, does not have a constant Thomas-Fermi screening up to  $q = 2k_f$  as exists in MLG and 2DEG [35].

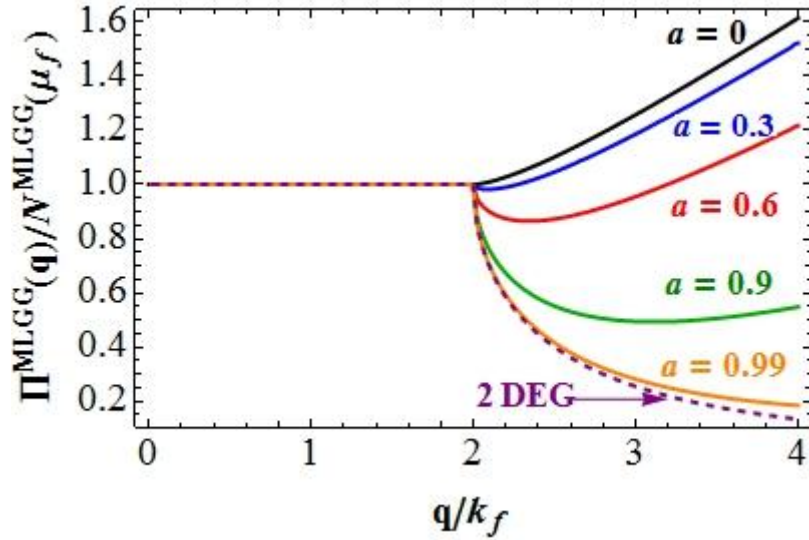


**Figure 2.3:** Calculated static polarization function of MLGG as a function of wave vector for different values of gap parameters.

The computed normalized polarization function as a function of  $q$  from Eq. (2.8) is plotted in Figure 2.3 for different gap values. As can be seen from Figure 2.3, the effect of introducing gap in electronic spectrum is almost unnoticeable for  $q \leq 2k_f$ , which means that the intraband and interband transitions almost cancel and the total polarization function is constant, similar to that in MLG [34]. But when  $q > 2k_f$  (large momentum transfer regime); (i) the magnitude of polarizability versus wave vector curve decreases on increasing the gap, at all  $q$ -values, and (ii) for  $a > 0.6$  the behaviour of polarizability versus wave vector curve for MLGG resembles to a great extent with that of 2DEG polarizability which is in stark contrast to MLG where the polarizability increases for  $q > 2k_f$ . This means that in MLGG the interband transitions dominate over the intraband transition for large wavevectors, suggesting that the scattering by the screened coulomb potential is much reduced due to enhanced screening in this limit. This also implies that for  $a = 0$ , polarizability (MLGG) shows relativistic characteristics while at  $a \approx 1$  it reflects the nonrelativistic nature of 2DEG caused by breaking of sublattice symmetry.

### 2.3.2 Electron-Impurity Scattering Rate as a Function of Energy

We attempted both analytical as well as numerical solutions of Eqs. (2.10)-(2.13). Numerical solutions have been worked out whenever analytical solutions are not possible. Integration over  $\theta$  in Eq. (2.10), for  $q \leq 2 k_f$ , where  $k_f = \sqrt{\pi \times 10^{12}}$  is Fermi wave vector, gives

$$\frac{\hbar}{\tau_{sl} \epsilon_f} = \frac{4 \alpha^2 y}{N} \left( \frac{\pi}{(4 \chi y)^2} - \frac{2 \alpha I_1}{(2 \chi y)^2} + \frac{\alpha^2 I_2}{(2 \chi y)^2} \right), \quad (2.18)$$

where  $\alpha = (4 e^2) / (\gamma k)$  is the dimensionless coupling constant. In obtaining Eq. (13), we have used the scaled variable;  $\chi = 1 - \pi \alpha / 8$ ,  $N = n_c / n_i$ , and normalized energy  $x = E / E_f$ .  $I_1$  and  $I_2$  are defined as;

$$I_1 = \frac{\pi (\alpha - \sqrt{\alpha^2 - (2 \chi x)^2})}{4 \chi x} + \frac{\sin^{-1} \left( \frac{2 \chi x}{\alpha} \right) \sqrt{\alpha^2 - (2 \chi x)^2}}{2 \chi x} - 1 \quad (2.19)$$

$$I_2 = \frac{1}{2 \chi x \alpha} - \frac{\pi}{2 (2 \chi x)^2} - \frac{2 \alpha \tan^{-1} \left( \frac{\alpha}{\alpha^2 - (2 \chi x)^2} \right)}{(2 \chi x)^2 \sqrt{\alpha^2 - (2 \chi x)^2}} \quad (2.20)$$

For  $q > 2 k_f$ , integral over  $\theta$  in Eq. (2.10) is not amenable to analytical solution and therefore numerical integral was made. The formalism developed in this study has better applicability for the case of  $n_i \leq n_c$ . We computed electron-impurity scattering rate as function of  $E$  for  $\alpha = 1.42$  and  $\chi = 0.42$ , at three different values of  $N (= 1, 2, 3)$ . The computed normalized scattering rate,  $\hbar / \tau^{\text{MLG}}(E) E_f$  is potted in Figure 2.4. As can be seen from Figure 2.4,  $\hbar / \tau^{\text{MLG}}(E)$  enhances monotonically for  $0 \leq E \leq E_f$  and attains a maximum value at around  $E \cong 1.56 E_f$ . It starts declining thereafter for higher values of  $E$ , at all values of  $N$ .

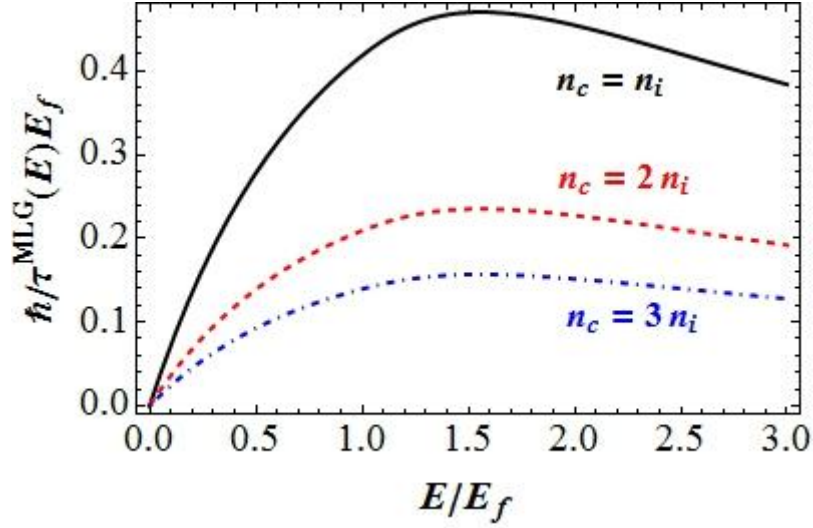


**Figure 2.4:** Normalized scattering rate of MLG,  $\hbar/\tau^{\text{MLG}}(E)E_f$  as a function of normalized energy  $E/E_f$ , for different impurity concentration,  $N = n_c/n_i$ .

On comparing our computed result on  $\hbar/\tau^{\text{MLG}}(E)$  with prior reported calculations of electron-impurity scattering rate for MLG, we find; (i) unlike earlier reported calculations,  $\hbar/\tau^{\text{MLG}}(E)$  does not exhibit maximum value at  $E = E_f$ , (ii)  $\hbar/\tau^{\text{MLG}}(E)$  shows strong dependence on  $E$  and it tends to zero when  $E$  goes to zero, (iii) the  $E$ -dependence of  $\hbar/\tau^{\text{MLG}}(E)$  is much stronger for  $E (\leq 2E_f)$  than for higher value of  $E$ , (iv) for higher values of energy, scattering rate tends to become less dependent on  $E$ , suggesting that a larger excitation energy ( $> 2E_f$ ) destroys electron-impurity scattering and (v) the scattering rate enhances on increasing impurity concentration,  $n_i$ . Prior reported calculations on conductivity, within Boltzmann transport theory, for MLG have used  $1/\tau^{\text{MLG}}(E_f)$  instead of  $\langle 1/\tau^{\text{MLG}}(E) \rangle$ , an averaged over all possible values of  $E$ , for comparing their theoretical results with experimental [25]. By looking at Figure 2.4 and on the basis of above discussions it can easily be said that this kind of comparison between theory and experiment is misleading and incorrect.

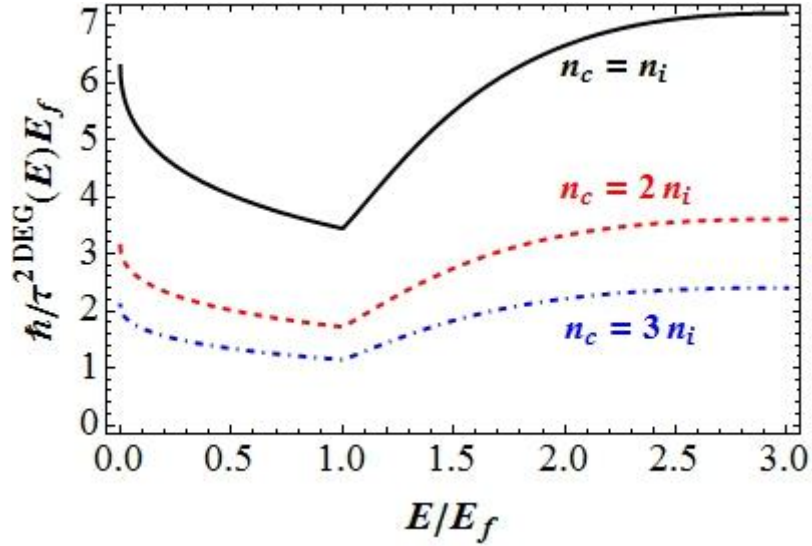


**Figure 2.5:** Normalized scattering rate of 2DEG,  $\hbar/\tau^{2\text{DEG}}(E) E_f$  as a function of normalized energy  $E/E_f$ , for different impurity concentration,  $N = n_c/n_i$ .

To provide a thorough understanding of electron-impurity scattering in MLG, we computed the electron-impurity scattering rate for 2DEG as well as for BLG with the use of Eqs. (2.11) and (2.12). We computed  $\hbar/\tau^{2\text{DEG}}(E)$  and  $\hbar/\tau^{\text{BLG}}(E)$  in terms of scaled variable;  $\beta = 2 m e^2/\hbar^2 k k_f$ ,  $N = n_c/n_i$ , and normalized energy  $x = E/E_f$ . Figure 2.5 displays our computed normalized electron-impurity scattering rate,  $\hbar/\tau^{2\text{DEG}}(E) E_f$  as a function of  $E$  for 2DEG (GaAs), which is modeled in terms of parameters;  $m = 0.067m_e$ , and  $\beta = 2.3755$  [38]. Figures 2.4 and 2.5 suggest that the  $E$ -dependence of electron-impurity scattering rate in MLG is entirely different than that in 2DEG.  $\hbar/\tau^{\text{MLG}}(E)$  increases, while  $\hbar/\tau^{2\text{DEG}}(E)$  declines with  $E$  in the range of  $0 \leq E \leq E_f$ . For  $E > E_f$   $\hbar/\tau^{\text{MLG}}(E)$  declines whereas  $\hbar/\tau^{2\text{DEG}}(E)$  increases with  $E$ . This difference in the nature of two scattering rates as function of  $E$  can be attributed to the difference in  $q$ -dependence of polarization function, quasi-particle energy dispersion relation and the density of states of MLG and 2DEG. As is known, quasi-particle energy varies linearly with wave vector in case of MLG, while it varies as quadratically with wave vector for 2DEG. The density of states is independent of  $E$  for

2DEG, while it varies linearly with  $E$  for MLG. The static polarization function,  $\Pi(q)$  of MLG exhibit entirely different behavior as a function of  $q$  than that of 2DEG, as can be seen from Figure 2.1 (b). Polarization functions of both MLG and 2DEG are independent of  $q$  for  $0 \leq q \leq 2k_f$ . However, polarization function increases linearly with  $q$  for MLG and declines quadratically for the 2DEG, for  $q > 2k_f$  as is displayed in Figure 2.1 (b). Equations (2.10) to (2.13) show that the electron-impurity scattering rate is inversely proportional to the square of static dielectric function that involves  $\Pi(q)$ . The increase of  $\hbar/\tau^{\text{MLG}}(E)$  with  $E$  for  $E \leq E_f$  is mainly contributed by  $E$ -dependence of  $N^{\text{MLG}}(E)$ . For  $E > E_f$ ,  $\epsilon^{\text{MLG}}(q)$  and  $N^{\text{MLG}}(E)$  contributes oppositely to  $\hbar/\tau^{\text{MLG}}(E)$  to give a declining behaviour of  $\hbar/\tau^{\text{MLG}}(E)$  versus  $E$ .

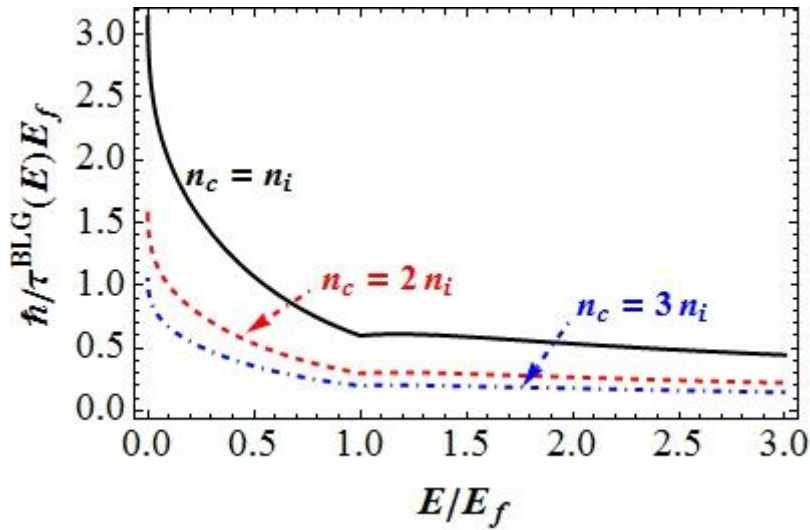


**Figure 2.6:** Normalized scattering rate of BLG,  $\hbar/\tau^{\text{BLG}}(E)E_f$  as a function of normalized energy  $E/E_f$ , for different impurity concentration,  $N = n_c/n_i$ .

Our computed electron-impurity scattering rate for BLG using Eq. (2.12) is plotted as a function  $E$  in Figure 2.6. For computation of results we used;  $m = 0.033m_e$ , and  $\beta = 1.17003$ . Nature of  $\hbar/\tau^{\text{BLG}}(E)$  versus  $E$  curves is very different from that of  $\hbar/\tau^{\text{MLG}}(E)$  and  $\hbar/\tau^{\text{2DEG}}(E)$  versus  $E$  curves, as can be seen from Figures. 2.4, 2.5 and 2.6. Unlike the

case of 2DEG,  $\hbar/\tau^{\text{BLG}}(E)$  exhibits continuous decline with  $E$ . However, a slight dip at around  $E = E_f$  can be seen from the Figure 2.6. It is interesting to note that though the polarization function for both MLG and BLG remains constant for  $E \leq 0.25 E_f$ ,  $\hbar/\tau^{\text{MLG}}(E)$  and  $\hbar/\tau^{\text{BLG}}(E)$  exhibit opposite behaviour with  $E$  for  $E$  up to  $E_f$ . The dip in  $\hbar/\tau^{\text{BLG}}(E)$  at around  $E = E_f$  could be attributed to a peak in polarization function of BLG at  $q = 2k_f$ . The nature of scattering rate with  $E$  does not alter on changing the value impurity concentration for MLG, 2DEG and BLG, as can be seen from Figures. 2.4, 2.5 and 2.6. For  $q < 2k_f$ , polarization function of BLG is initially constant with  $q$ , and then it increases sharply for  $q$  up to  $2k_f$  because of the enhanced backscattering in BLG, which is not the case of MLG and 2DEG.

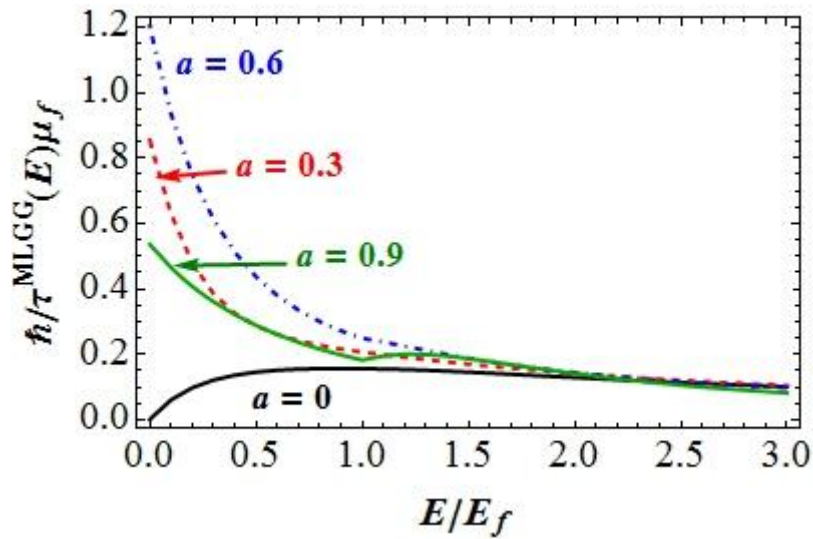


**Figure 2.7:** Normalized scattering rate of MLGG,  $\hbar/\tau^{\text{MLGG}}(E)\mu_f$  as a function of normalized energy ( $E/E_f$ ), for different gap parameters ( $a = \Delta/\mu_f$ ). Here we used dimensionless coupling constant  $\alpha = 1$  and scaled impurity concentration  $N = 1$ .

Our computed  $\hbar/\tau^{\text{MLGG}}(E)\mu_f$  as a function of  $E$  at different values of  $a$  ( $0 \leq a < 1$ ) for zero temperature is displayed in Figure 2.7. As can be seen from Figure 2.7,  $\hbar/\tau^{\text{MLGG}}(E)\mu_f$  for zero gap (gapless graphene); (i) goes to zero for  $E \rightarrow 0$ , (ii) exhibits a maximum at around

$E \sim 0.6 E_f$ , and (iii) decreases monotonically thereafter for higher  $E$ -values. For non-zero values of gap ( $a = 0.3, 0.6, 0.9$ ),  $\hbar/\tau^{\text{MLGG}}(E)\mu_f$  approaches a finite value at  $E = 0$  and the nature of  $\hbar/\tau^{\text{MLGG}}(E)\mu_f$  versus  $E$  curve changes on increasing  $a$ . At higher values of  $a$ ,  $\hbar/\tau^{\text{MLGG}}(E)\mu_f$  shows an inverted behavior to that seen at  $a = 0$  for  $E < 0.6 E_f$ . The nature of  $\hbar/\tau^{\text{MLGG}}(E)\mu_f$  versus  $E$  curve strongly depends on  $a$  for lower values of  $E$ , which is not the case for higher values of  $E$ . This distinctly different behavior of  $\hbar/\tau^{\text{MLGG}}(E)\mu_f$  versus  $E$  for  $a = 0$  from that for  $a \neq 0$ , can be attributed to the difference in energy dispersion relation and density of states for the two cases. Gapless graphene exhibits linear energy dispersion relation and zero density of states at Dirac points, which is not the case for gapped graphene. On comparing our computed results for gapped graphen ( $a \neq 0$ ) with those for BLG, we find that nature of  $\hbar/\tau^{\text{MLGG}}(E)\mu_f$  as a function of  $E$  curve is very similar to that of BLG, when  $0.9 \leq a < 1$ .

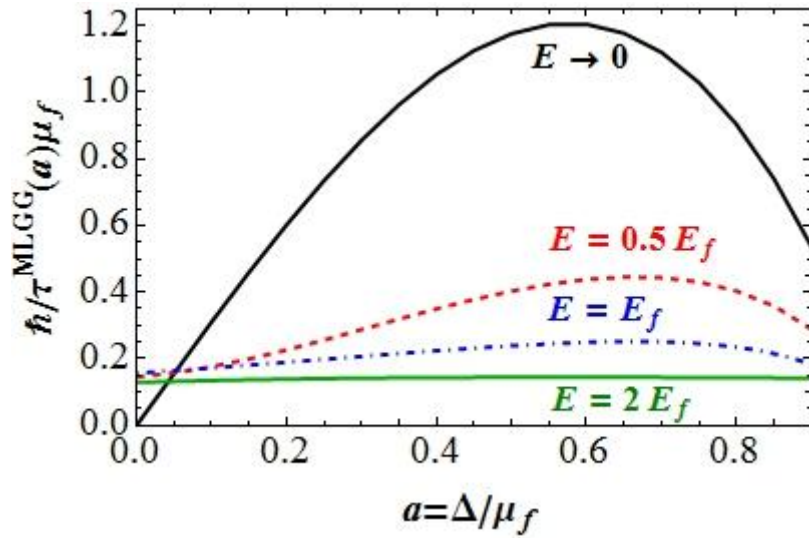


**Figure 2.8:** Normalized scattering rate of MLGG,  $\hbar/\tau^{\text{MLGG}}(a)\mu_f$  as a function of gap parameter ( $a = \Delta/\mu_f$ ), for different values of normalized energy ( $E/E_f$ ). Here we used dimensionless coupling constant  $\alpha = 1$  and scaled impurity concentration  $N = 1$ .

The effect of opening of gap in electronic states on electron-impurity scattering can be understood from computed  $\hbar/\tau^{\text{MLGG}}(a)\mu_f$  as a function of gap parameter ( $a$ ) at different

values of normalized energy ( $E/E_f$ ), displayed in Figure 2.8. It can be seen that behavior of  $\hbar/\tau$  verses  $a$  curve for  $E \rightarrow 0$  is distinctly different from that at  $E = (0.5, 1 \& 2)E_f$  when  $0 \leq a \leq 0.6$ . The  $a$ -dependence of  $\hbar/\tau^{\text{MLGG}}(a)\mu_f$  for  $E \rightarrow 0$  is much stronger than that for  $E = (0.5, 1 \& 2)E_f$ . This clearly suggests that; (i)  $\hbar/\tau^{\text{MLGG}}(a)\mu_f$  goes to zero when both  $E$  and  $a$  are zero, and (ii) nature of electron-impurity scattering in the regime of  $E$  and  $a$  when one of these is zero and both are smaller than Fermi energy is entirely different than that for the cases when both  $E \neq 0$  and  $a \neq 0$ . We thus find that opening of energy gap in electronic spectrum of single layer graphene, which changes density of state and energy dispersion relation, plays an important role in determining transport properties of graphene.

### 2.3.3 Electron-Impurity Scattering Rate as a Function of Impurity Concentration

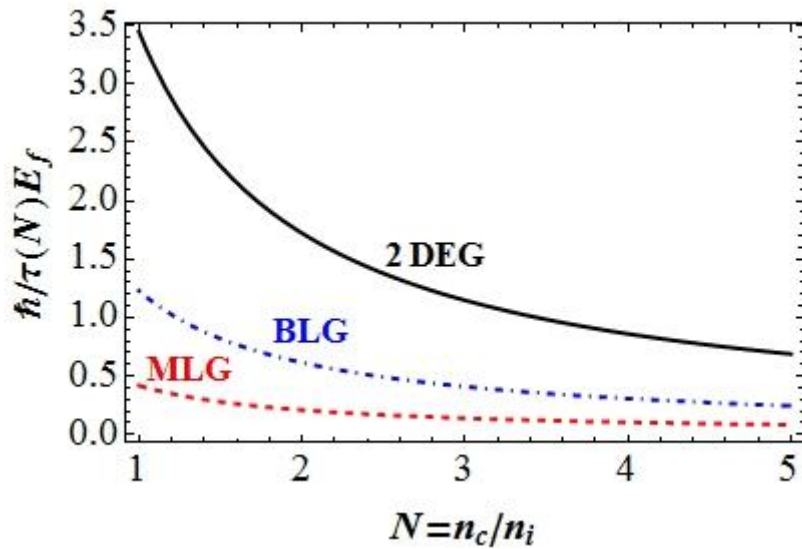


**Figure 2.9:** Normalized scattering rate,  $\hbar/\tau(N)E_f$  is plotted as a function of  $N = n_c/n_i$ , for MLG (red-dashed), BLG (blue-dot dashed) and 2DEG (black-solid). Here we used dimensionless coupling constant  $\alpha = 1.48$  and  $E = E_f$ .

Figure 2.9 depicts variation of scattering rate as a function of impurity concentration at Fermi energy for MLG, BLG and 2DEG. As can be seen from the figure, it enhances on increasing

impurity concentration for all the cases. It is interesting to note from Figure 2.9 that scattering rate does not vary linearly with change in impurity concentration. High impurity concentration giving rise to a sharp increase in scattering rate, as can be observed from figure.  $\hbar/\tau(N)E_f$  is not plotted for  $n_i \geq n_c$  because at very high value of impurity concentration validity of Boltzmann transport approximation comes under question mark.

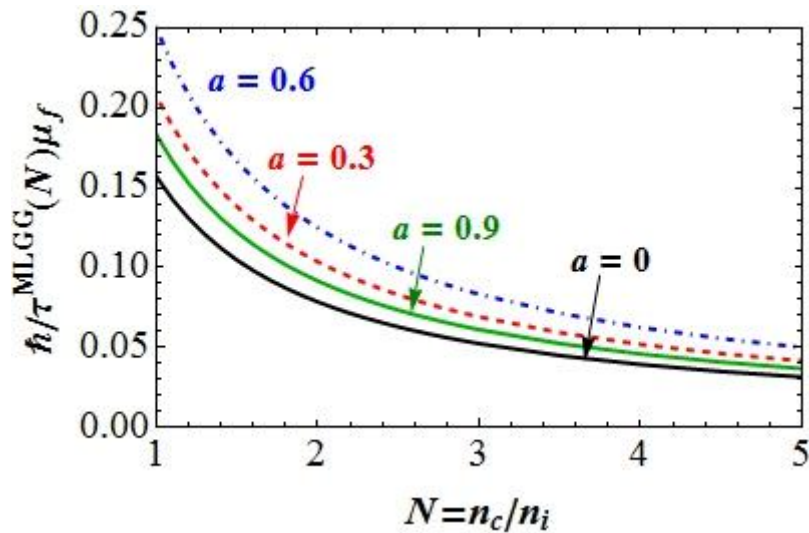


**Figure 2.10:** Normalized scattering rate,  $\hbar/\tau^{\text{MLGG}}(N)\mu_f$  of MLGG as a function of  $N = n_c/n_i$  for different gap parameters ( $a = \Delta/\mu_f$ ). Here we used dimensionless coupling constant  $\alpha = 1$  and  $E = E_f$ .

Figure 2.10 depicts variation of scattering rate of MLGG as a function of impurity concentration at Fermi energy for different values of gap parameters. As can be seen from the figure, it enhances scattering rate with an increasing impurity concentration for all values of gap parameters. Our observation from Fig. 2.8 that the scattering rate enhances on increasing gap parameters up to  $a \approx 0.65$  and gradually decreases for higher values can also be confirmed from the scattering rate curves shown in Fig. 2.10 where, the scattering rate curve calculated for  $a = 0.9$  is laying lower than the scattering rate curve calculated at  $a = 0.6$ .

The electron-phonon interaction can play an important role in determining transport properties of BLG as well as MLG [39, 40]. It has been shown that electron-phonon

interaction renormalizes the mass of electron in term of electron-phonon coupling strength in BLG. As compared to graphite, larger renormalization of Fermi velocity due to electron-phonon interaction has been found in BLG [39]. Density of states of BLG, which appears in formalism of  $\hbar/\tau^{\text{BLG}}(E)$ , involves effective mass of electron. It can therefore be inferred that electron-phonon interaction will change the magnitude of  $\hbar/\tau^{\text{BLG}}(E)$ . However, all behavior of  $\hbar/\tau^{\text{BLG}}(E)$  with  $E$  and  $n_i$  will remain unaltered. Also, at very low temperatures ( $T \approx 0$ ), electron-electron interactions and the electron-phonon interactions are not effective and therefore electron-impurity scattering dominates the electronic scatterings [41].

## 2.4 References

- [1] Y. Zhang *et al.*, Nature **438**, 201 (2005).
- [2] K. S. Novoslov *et al.*, Science **306**, 666 (2004).
- [3] T. Ando, J. Phys. Soc. Jpn. **74**, 777 (2005).
- [4] E. A. Taft and H. R. Philipp, Phys. Rev. A **138**, 187 (1965).
- [5] J. Gonzalez, F. Guinea and M. A. H. Vozmediano, Nucl. Phys. B **424** (1994).
- [6] J. Gonzalez, F. Guinea and M.A.H. Vozmediano, Phys. Rev. B **59**, 2474 (1999).
- [7] D. P. DiVincenzo and E. J. Mele, Phys. Rev. B **29**, 1685 (1984).
- [8] T. Ando and T. Nakanishi, J. Phys. Soc. Jpn. **67**, 1704 (1998).
- [9] K. S. Novoselov *et al.*, Proc. Natl. Acad. Sci. U.S.A. **102**, 10451 (2005).
- [10] K. S. Novoslov *et al.*, Nature **438**, 197 (2005).
- [11] A. H. Castro Neto *et al.*, Rev. Mod. Phys. **81**, 109 (2009).
- [12] I. Gierz *et al.*, Nano Lett. **8**, 4603 (2008).
- [13] D. A. Siegel *et al.*, Appl. Phys. Lett. **93**, 243119 (2008).
- [14] S. Y. Zhou *et al.*, Physica E **40**, 2642 (2008).
- [15] G. Giovannetti *et al.*, Phys. Rev. B **76**, 073103 (2007).
- [16] E. McCann, Phys. Rev. B **74**, 161403 (2006).
- [17] H. Min *et al.*, Phys. Rev. B **75**, 155115 (2007).
- [18] T. Ando and M. Koshino, J. Phys. Soc. Jpn. **78**, 034709 (2009).
- [19] T. Ando and M. Koshino, J. Phys. Soc. Jpn. **78**, 104716 (2009).

- [20] P. Cea, Mod. Phys. Lett. B **26**, 1250084 (2012).
- [21] R. C. Tatar and S. Rabii, Phys. Rev. B **25**, 4126 (1982).
- [22] M. I. Katsnelson and A. K. Geim, Phil. Trans. R. Soc. A **366**, 195 (2008).
- [23] G. Trambly de laissardi`ere and D. Mayou, Mod. Phys. Lett. B **25**, 1019 (2011).
- [24] A. Qaiumzadeh and R. Asgari, Phys. Rev. B **79**, 075414 (2009).
- [25] T. Ando, J. Phys. Soc. Jpn. **75**, 074716 (2006).
- [26] K. Nomura and A. H. Mac Donald, Phys. Rev. Lett. **96**, 256602 (2006).
- [27] M. I. Katsnelson, Mater. Today **10**, 20 (2007).
- [28] E. H. Hwang, S. Adam and S. D. Sarma, Phys. Rev. Lett. **98**, 186806 (2007).
- [29] V. V. Cheianov and V. I. Falko, Phys. Rev. Lett. **97**, 226801 (2006).
- [30] S. Adam *et al.*, Proc. Natl. Acad. Sci. U.S.A. **104**, 18392 (2007).
- [31] S. D. Sarma and E. H. Hwang, Phys. Rev. Lett. **83**, 164 (1999).
- [32] T. Ando, A. B. Fowler and F. Stern, Rev. Mod. Phys. **54**, 437 (1982).
- [33] M. Lv and S. Wan, Phys. Rev. B. **81**, 195409 (2010).
- [34] E. H. Hwang and S. D. Sarma, Phys. Rev. B. **75**, 205418 (2007).
- [35] E. H. Hwang and S. D. Sarma, Phys. Rev. Lett. **101**, 156802 (2008).
- [36] P K Pyatkovskiy, J. Phys.: Condens. Matter **21**, 025506 (2009).
- [37] S. D. Sarma and E. H. Hwang, Phys. Rev. B **69**, 195305 (2004).
- [38] P. Lawaetz, Phys. Rev. B. **4**, 3460 (1971).
- [39] C. H. Park *et al.*, Nano Lett. **8**, 4229 (2008).
- [40] A. Das, B. Chakraborty and A. K. Sood, Mod. Phys. Lett. B **25**, 511 (2011).

[41] M. Shen, *“Low Temperature Electron-Phonon Interaction in Disordered Metal Thin Films and Applications to Fast, Sensitive Sub-Millimeter Photon Sources and Detectors”*, Ph.D. Thesis, Yale University (2005).